

Cascaded deep UV and blue LEDs with integrated GaN tunnel junction

Amina Hafeez, Muhammad Usman, Hazrat Ali, Jamshad Bashir, and Zoya Noor

Citation: Chin. Phys. B, 2026, 35 (**5**): 057302. DOI: 10.1088/1674-1056/ae32fd
http://cpb.iphy.ac.cn; http://iopscience.iop.org/cpb

What follows is a list of articles you may be interested in

Hydrothermal synthesis and nonvolatile resistive switching properties of α-Fe_2O_3 nanosheet arrays

Zhi-Qiang Yu(余志强), Xin-Wei Zhao(赵新为), Bao-Sheng Liu(刘宝生), Tang-You Sun(孙堂友), and Zhi-Mou Xu(徐智谋)

Chin. Phys. B, 2026, 35 (**1**): 017302. DOI: 10.1088/1674-1056/adee88

Scanning tunneling microscopy study on symmetry breaking of charge density wave in FeGe

Jiakang Zhang(张嘉康), Ziyuan Chen(陈子元), Xueliang Wu(吴学良), Mingzhe Li(李明哲), Yuanji Li(李元骥), Ruotong Yin(尹若彤), Jiashuo Gong(巩佳硕), Shiyuan Wang(王适源), Aifeng Wang(王爱峰), Dong-Lai Feng(封东来), and Ya-Jun Yan(闫亚军)

Chin. Phys. B, 2025, 34 (**4**): 047303. DOI: 10.1088/1674-1056/adb389

Peak structure in the interlayer conductance of Moiré superlattices

Yizhou Tao(陶懿洲), Chao Liu(刘超), Mingwen Xiao(肖明文), and Henan Fang(方贺男)

Chin. Phys. B, 2024, 33 (**10**): 107301. DOI: 10.1088/1674-1056/ad655b

Field induced Chern insulating states in twisted monolayer-bilayer graphene

Zhengwen Wang(王政文), Yingzhuo Han(韩英卓), Kenji Watanabe, Takashi Taniguchi, Yuhang Jiang(姜宇航), and Jinhai Mao(毛金海)

Chin. Phys. B, 2024, 33 (**6**): 067301. DOI: 10.1088/1674-1056/ad3b8a

Design optimization of a silicon-germanium heterojunction negative capacitance gate-all-around tunneling field effect transistor based on a simulation study

Weijie Wei(魏伟杰), Weifeng Lü(吕伟锋), Ying Han(韩颖), Caiyun Zhang(张彩云), and Dengke Chen(谌登科)

Chin. Phys. B, 2023, 32 (**9**): 097301. DOI: 10.1088/1674-1056/acaa2c

---

Cascaded deep UV and blue LEDs with integrated GaN tunnel junction

Amina Hafeez[1], Muhammad Usman[2,†], Hazrat Ali[1,‡], Jamshad Bashir[2], and Zoya Noor[2]

[1] *Department of Physics, Abbottabad University of Science and Technology, Khyber Pakhtunkhwa, Pakistan*

[2] *Faculty of Sciences, Ghulam Ishaq Khan Institute of Engineering Sciences and Technology, Topi,* 23460, *Khyber Pakhtunkhwa, Pakistan*

(Received 19 September 2025; revised manuscript received 15 December 2025; accepted manuscript online 4 January 2026)

The growing demand for reliable sterilization methods, coupled with the spread of COVID-19, has driven exploration of the use of deep ultraviolet (DUV) radiation for disinfection purposes. Given that exposure to highly energetic DUV radiation poses a significant risk to the eyes and skin, portable sterilizing equipment must emit both visible and DUV wavelengths to simultaneously indicate its operation and perform sterilize. In this paper, we explore the effect of the tunnel junction in cascading visible and ultraviolet active regions instead of the cascade region. In our reference device, two $Al_xGa_{1-x}N$ layers are used to facilitate carrier movement from one active region to another, but this does not work effectively due to the presence of greater barriers for holes and electrons. Introducing a tunnel junction reduces these barriers; consequently, the radiative recombination rate is increased by a factor of 2.2, while the emission intensity is increased by factors of 1.3 and 2.7 for ultraviolet and blue wavelengths, respectively.

Keywords: tunneling, quantum wells, radiative recombination, III–V semiconductors

PACS: 73.43.Jn, 68.65.Fg, 72.20.Jv, 78.66.Fd

DOI: 10.1088/1674-1056/ae32fd **CSTR:** 32038.14.CPB.ae32fd

1. Introduction

Electroluminescent devices such as light-emitting diodes (LEDs) and laser diodes (LDs) are replacing traditional light sources due to their tunable wavelength, minimal power consumption, long lifetime, eco-friendliness, and compactness.[1] Deep ultraviolet (DUV) LEDs do not need any warmup time, as they can turn on and off instantly.[2] DUV LEDs have many potential applications, such as treating cancer, therapies, sanitation, air and water purification,[3] surface disinfection, data storage,[4] food purification, and sterilization.[5,6] GaN and AlN have direct bandgap values of 3.4 eV and 6.2 eV, respectively.[7] Their bandgaps can be tuned by producing ternary and quaternary alloys, such as AlGaN and AlGaInN.[8] Owing to this unique tunability, III–N-based LEDs can be engineered to emit across the entire visible spectrum by altering the composition of the alloy. Extensive research into III–N has been conducted over the last two decades because of these outstanding features. Despite these characteristics, III–N LEDs still encounter some issues, including low output power (LOP), low extraction efficiency (LEE),[9] the quantum-confined Stark effect (QCSE),[10] electron leakage,[11] poor hole injection,[12] and poor wall-plug efficiency (WPE). To improve the optoelectronic performance of III–N-based LEDs, numerous novel devices have been proposed in the literature, such as graded and step-graded electron blocking layers (EBLs),[13] single and double quantum barriers (QBs),[14] engineering a last quantum barrier (LQB)[15] instead of an EBL, p-GaN/AlGaN superlattices,[16] single and double triangular QBs,[17] inverted-V-shaped EBLs,[18] non-square quantum wells (QWs),[19] structures without EBLs featuring designed final QBs,[20] and tunnel junctions (TJs) for better hole injection.[21] When DUV and blue QWs are integrated within a single monolithic LED, the device can simultaneously enable sterilization, sensing, and visible-light functionality in a compact system.

The DUV emission is crucial for germicidal disinfection, water and air purification, and high-energy fluorescence excitation. The blue emission provides visible feedback, optical alignment, calibration, and secondary fluorescence excitation, which are essential in practical devices. This dual-emission design eliminates the need for multiple light sources or phosphors, reducing system size, power consumption, and optical complexity. Such integrated DUV–blue LEDs are particularly valuable for portable disinfection units, lab-on-chip diagnostics, biomedical sensing, and smart optoelectronic platforms.[22,23] Recently, DUV and visible LEDs have been monolithically integrated via a cascade region to reduce electron leakage in sterilization applications. Following the COVID-19 outbreak, the requirement for disinfection and sterilization has increased. However, the prolonged and excessive use of high-radiation DUV LEDs poses hazards to the skin and eyes.[24,25] To address these issues, a blue LED is monolithically integrated with a DUV LED during the packaging process; this approach reduces both integration costs and fab-

†Corresponding author. E-mail: m.usman@giki.edu.pk

‡Corresponding author. E-mail: yamanuom@gmail.com

© 2026 Chinese Physical Society and IOP Publishing Ltd. All rights, including for text and data mining, AI training, and similar technologies, are reserved.

rication processes. According to the research literature, TJs are utilized in two different ways in III–N-based LEDs. First, TJs are used for hole injection by replacing the p-GaN contact layer,[26] which increases current injection efficiency. Secondly, a TJ can be employed to stack multiple quantum wells (MQWs),[27,28] thus enhancing the carrier concentration in the QWs, improving radiative recombination.[29] In this paper, we describe the construction of a unique n^+/p^+ GaN TJ sandwiched between blue and DUV active regions. The electron flux, hole flux, radiative recombination rate, internal quantum efficiency (IQE), and electron and hole concentrations are significantly increased in our device through multiple recombination processes in the vertically stacked active region. We believe that TJ-based dual LEDs will not only increase device performance but also reduce fabrication costs in the future.

2. Device characteristics

In this paper, we numerically investigate two structures at a temperature of 300 K: the reference device, named LED-JI,[30] and the proposed device, named LED-JII (see Fig. 1). LED-JI contains an n-$Al_{0.50}Ga_{0.50}N$ layer with a thickness of 2000 nm (Si: 5×10^{18} cm^{-3}), followed by a DUV active region consisting of four undoped $Al_{0.4}Ga_{0.6}N$ QWs, each with a thickness of 3 nm, which are placed between five undoped 10 nm thick $Al_{0.5}Ga_{0.5}N$ quantum barriers (QBs). After this active region, we have a cascade region consisting of 10 nm of ungraded p-$Al_{0.65}Ga_{0.35}N$ (Mg: 7×10^{19}) and a 10 nm graded p-$Al_{0.65-0.1}Ga_{0.35-0.9}N$ (Mg: 7×10^{19}) layer, where the ungraded layer functions as an EBL and the graded layer facilitates carrier mobility. Two intrinsic $In_{0.15}Ga_{0.85}N$ QWs succeed the cascade region with a thickness of 3 nm, along with three 10 nm thick GaN QBs. A 200 nm p-GaN (Mg: 7×10^{19}) hole injection layer is used to cap the structure. LED-JII and LED-JI are similar, except that the cascade region is replaced with an n^+-GaN/p^+-GaN TJ.[31] The doping concentration in both the n^+ and p^+ layers is 1×10^{20} cm^{-3}. We used the commercially available simulator SiLENSe for the numerical simulation of the devices under discussion. Three models are used for the electron–hole recombination in the MQW active region, namely the Shockley–Read–Hall (SRH) model and the Auger model for non-radiative transitions, and the bimolecular recombination model for radiative transitions. The radiative recombination-based IQE is obtained by integrating the radiative recombination from the whole LED structure. For the other parameters of the ternary alloys, Vegard's law is utilized by the simulator. Incomplete ionization of dopants is introduced by the incomplete model, while piezoelectric and spontaneous polarizations are introduced by the polar model. The coefficient for SRH recombination is set to 1×10^{-9} s, the coefficient for Auger recombination is 1×10^{-31} cm$^6\cdot$s^{-1}, and the coefficient for radiative recombination is obtained from the extent of the overlap in the hole and electron wave functions.[32] The parameters for III–N compounds are obtained from Ref. [33]. The size of the mesh for the QWs is kept at 0.1 nm; for all other layers, it is 2 nm, while the depth of the contact is 2 nm. The conduction and valence band offsets for AlGaN/GaN are 7:3, whereas for InGaN/GaN, they are 6.5:3.5, respectively.

Table 1. Spontaneous and piezoelectric polarization constants, lattice constants and activation energies.

Property	AlN	GaN	InN
C_{11} (GPa)	395	375	225
C_{12} (GPa)	140	140	110
C_{13} (GPa)	115	105	95
C_{33} (GPa)	395	395	200
e_{15} (C·m^{-2})	–0.48	–0.27	–0.18
e_{31} (C·m^{-2})	–0.58	–0.33	–0.22
e_{33} (C·m^{-2})	1.55	0.65	0.43
Spontaneous polarization (C·m^{-2})	–0.081	–0.02	–0.032
a (nm)	0.3112	0.3188	0.354
c (nm)	0.4982	0.5186	0.5705
Activation energy, donor (meV)	13	13	13
Activation energy, acceptor (meV)	470	170	170

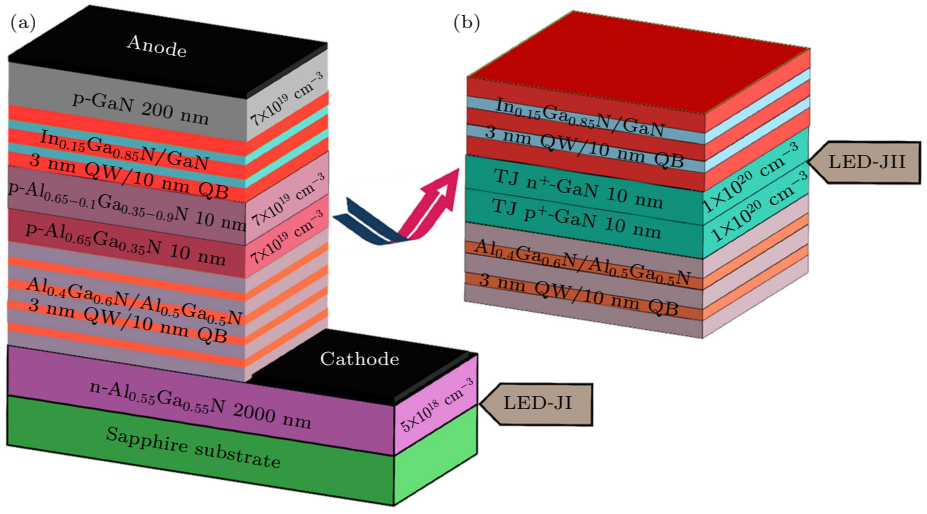


Fig. 1. (a) DUV–blue reference device. (b) TJ that replaces the cascade region in the proposed device.

Table 2. Device characteristics.

Device structure	SRH (ns)	Auger ($cm^{-6}\cdot s$)	Dopants (cm^{-3})		Mobility ($cm^2\cdot V^{-1}\cdot s^{-1}$)		Thickness (nm)	
			Si	Mg	Hole	Electron	LED JI	LED-JII
n-$Al_{0.50}Ga_{0.50}N$	1	1×10^{-31}	5×10^{18}	Nil	10	100	2000	2000
$Al_{0.5}Ga_{0.5}N$ QB	1	1×10^{-31}	Nil	Nil	10	100	10	10
$Al_{0.4}Ga_{0.6}N$ QW	1	1×10^{-31}	Nil	Nil	10	100	3	3
p-$Al_{0.65}Ga_{0.35}N/n^+$-GaN	1	1×10^{-31}	1×10^{20}	7×10^{19}	10	100	10	10
p-$Al_{0.65-0.1}Ga_{0.35-0.9}N/p^+$-GaN	1	1×10^{-31}	Nil	$7\times10^{19}/1\times10^{20}$	10	100	3	3
GaN QBs	1	1×10^{-31}	Nil	Nil	10	100	10	10
$In_{0.15}Ga_{0.85}N$ QW	1	1×10^{-31}	Nil	Nil	10	100	3	3
p-GaN	1	1×10^{-31}	Nil	7×10^{19}	10	100	200	200

3. Results and discussion

The electron and hole current densities of LED-JI and LED-JII at a current density of 300 $A\cdot cm^{-2}$ are shown in Figs. 2(a) and 2(b). The electron current densities in LED-JI and LED-JII are 112 $A\cdot cm^{-2}$ and 282 $A\cdot cm^{-2}$, respectively, as shown in Fig. 2(a). By incorporating the TJ electron flux from the DUV active region into the blue, the electron current density is increased by 2.52 times in the proposed LED. The reason for this enhancement in electron current density is the reduction in the conduction band barrier height of the LQB of the DUV wells. Figure 2(b) depicts the hole fluxes in LED-JI and LED-JII. The hole current densities in LED-JI and LED-JII are 169 $A\cdot cm^{-2}$ and 203 $A\cdot cm^{-2}$, respectively. The hole current density is enhanced by 1.2 times from the blue active region to the UV region in LED-JII. The reduced valence band hindrance is responsible for the increase in hole current density from the blue to DUV QWs.

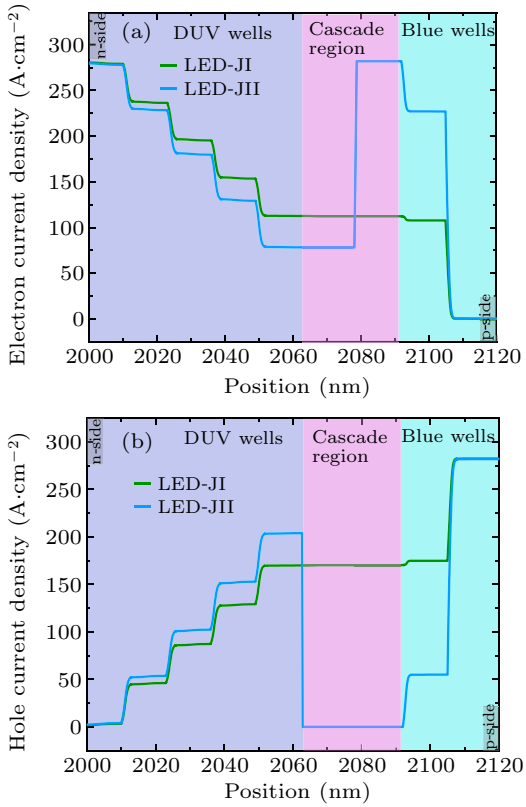


Fig. 2. Comparison of the (a) electron current density (b) hole current density of the devices under discussion.

To explore the barrier widths, calculated band profiles are presented in Figs. 3(a) and 3(b). The energy band profile of LED-JI, shown in Fig. 3(a), represents the barrier heights for electrons and holes, which are 298 meV and 350 meV, respectively. For multiwavelength LEDs, we are interested in the reduction of both barrier heights for better carrier dynamics. Keeping this in mind, in LED-JII, we introduced a GaN TJ instead of the cascade region. This completely removes the electron blocking behavior and reduces the valence band barrier to 310 meV. Thus, in LED-JII, the carriers can easily move through the active regions.

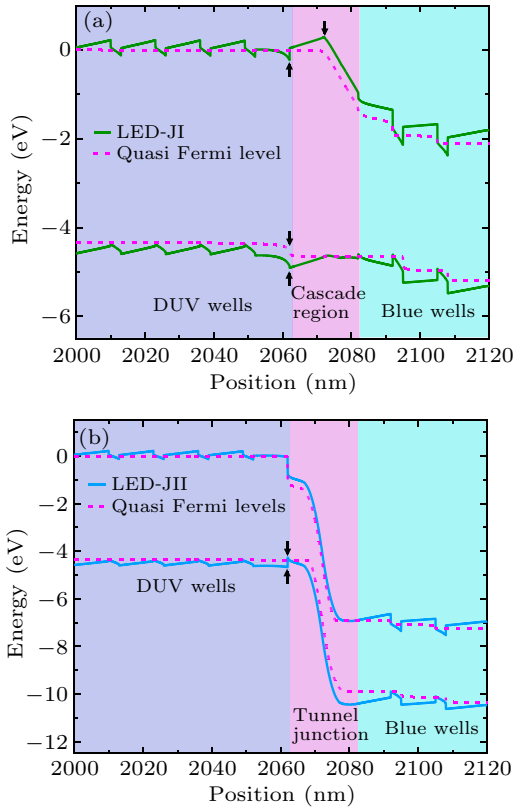


Fig. 3. Calculated energy band profiles of (a) LED-JI and (b) LED-JII.

To determine the effect of the reduced barriers on the carriers, a comparison of the concentrations of electrons and holes for both LEDs is displayed in Figs. 4(a) and 4(b). In the DUV wells of LED-JII, the electron concentration is enhanced by 3.4% compared to that of LED-JI, as shown in Fig. 4(a), and the electron concentration in the final DUV QW is decreased

in LED-JII due to the reduced conduction band barrier. In contrast, a significant 33.5% increase in electron concentration is observed in the blue QWs of LED-JII. Conversely, in the DUV QWs of LED-JII, the hole concentration is 7% higher than that in LED-JI, as can be observed from Fig. 4(b). While the hole concentration in the blue QWs is reduced, this reduction in hole concentration does not have any significant effect on the IQE because the electron concentration is much higher in the blue QWs, leading to higher radiative recombination, as discussed below.

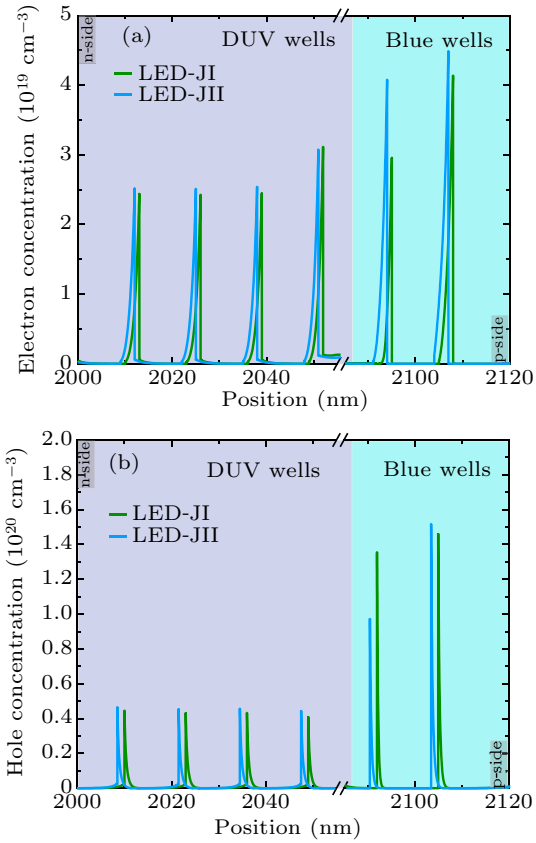


Fig. 4. Comparison of calculated (a) electron concentrations (b) hole concentrations at 300 A·cm^{-2}.

As is evident from the band diagram and carrier concentration graphs, the TJ facilitates carrier mobility. Therefore, a radiative recombination analysis was performed, as displayed in Fig. 5(a). LED-JII has a radiative recombination rate 2.2 times than that of LED-JI as it has more electrons and holes. Based on radiative recombination, the calculated IQEs are presented in Fig. 5(b). This comparison of the IQEs for both LEDs indicates that the IQE of LED-JII is 1.2 times higher than that of LED-JI and decreases with increasing current.

A comparison of output internal spontaneous emission intensities is presented in Fig. 6. The emission intensity from the DUV QWs of LED-JII is 31% greater than that of LED-JI, and a much more significant increase in spontaneous emission intensity is observed from the blue QWs of LED-JII, which is 2.7 times higher than that of LED-JI. The full width at half maximum (FWHM) of the peak at 278 nm is 5.49 nm in LED-JI and 5.47 nm in LED-JII, whereas the FWHM of the peak at 422 nm is 12.75 nm in LED-JI and 13.13 nm in LED-JII. In both emissions, the FWHM is approximately the same. This increase in emission intensity is associated with the significant increase in radiative recombination. The peak at 278 nm corresponds to the DUV regime, while the peak at 422 nm corresponds to the blue spectral regime.

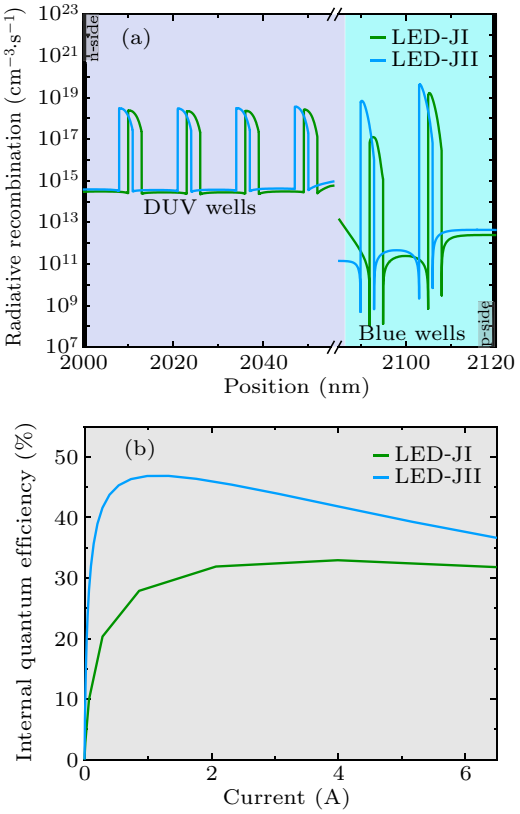


Fig. 5. Calculated (a) radiative recombination rate (b) IQE.

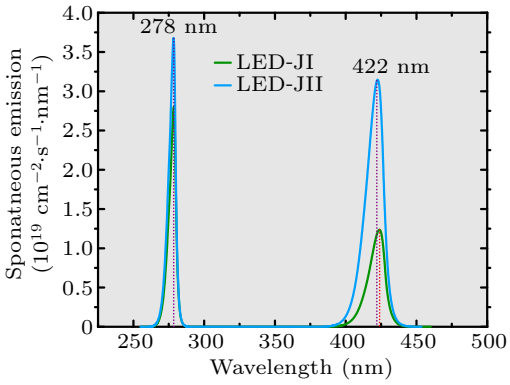


Fig. 6. Emission intensities of LED-JI and LED-JII.

The *J*–*V* characteristics of LED-JI and LED-JII are shown in Fig. 7. LED-JI exhibits a turn-on voltage of 4.6 V, which is significantly lower than that of LED-JII. However, despite the low operating voltage, the carrier concentration in the QWs of LED-JI does not notably increase with applied bias, resulting in a limited radiative recombination rate. Consequently, LED-JI demonstrates a lower IQE and a weaker

emission intensity, indicating inefficient carrier confinement and an imbalance in carrier injection within the active region. In contrast, LED-JII exhibits a higher turn-on voltage of approximately 8 V, which is nearly double that of LED-JI. This increase in turn-on voltage originates from the incorporation of the TJ, which increases series resistance and introduces an additional tunneling barrier and voltage drop across the n^+/p^+ GaN interface.[28] The area-specific series resistance of LED-JI is 1.39×10^{-4} Ω·cm^2, whereas for LED-JII, it is 2.86×10^{-4} Ω·cm^2, and the differential resistance for the TJ is 1.2×10^{-3} Ω·cm^2. Although a higher bias is required to initiate conduction, once the device is turned on, the TJ significantly enhances carrier injection into the QWs, leading to increased carrier concentration, a higher radiative recombination rate, and improved IQE.

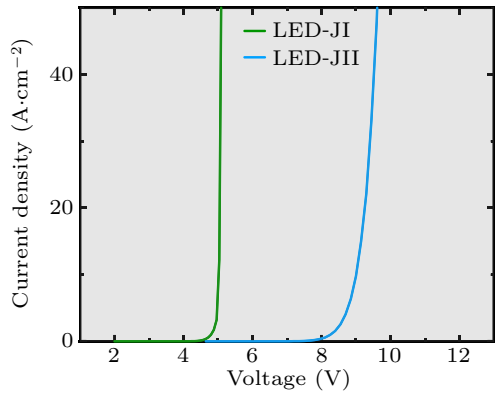


Fig. 7. Emission intensities of LED-JI and LED-JII.

4. Conclusions

In this paper, we numerically analyze the effect of the GaN-based TJ on monolithically integrated DUV–blue LEDs. LED-JII, with an n^+/p^+ GaN TJ, improves carrier transport, particularly the electron and hole injection into the blue and DUV active regions. As a result of this optimized carrier injection, the radiative recombination rate is enhanced, leading to a significant increase in emission intensity and an IQE boost of 1.2 times compared to that of LED-JI. Additionally, emission intensities in both the DUV and blue spectral regimes are significantly elevated, making the dual-wavelength LED highly efficient and well-suited for sterilization and disinfection applications. The proposed TJ-integrated structure not only boosts electro-optic performance but also simplifies fabrication processes, offering a promising pathway toward the next generation of cost-effective, high-performance multiwavelength LEDs.

Acknowledgement

The authors are obliged to the Ghulam Ishaq Khan Institute of Engineering Sciences and Technology (Pakistan) for providing the resources needed for this research.

References

[1] Usman M, Malik S, Hussain M, Ali S, Saeed S and Anwar A R 2022 *Optical Review* **29** 498
[2] Kuo Y K, Chang J Y, Chang H T, Chen F M and Shih Y H 2016 *IEEE J. Quantum Electron.* **53** 3300106
[3] Floyd R, Gaevski M, Hussain K, *et al*. 2021 *Appl. Phys. Express* **14** 084002
[4] Ma Z, Almalki A, Yang X, *et al*. 2020 *J. Alloys Compd.* **845** 156177
[5] Kowalski W 2010 *Ultraviolet Germicidal Irradiation Handbook* (New York: Springer)
[6] Bolton J R and Cotton C A 2008 *The Ultraviolet Disinfection Handbook* (Denver: American Water Works Association)
[7] Das S, Lenka T R, Talukdar F A, *et al*. 2023 *Micromachines* **14** 1926
[8] Gaska R, Chen C, Yang J, *et al*. 2002 *Appl. Phys. Lett.* **81** 4658
[9] Lobo-Ploch N, Mehnke F, Sulmoni L, *et al*. 2020 *Appl. Phys. Lett.* **117** 111102
[10] Tao G, Zhao X and Zhou S 2021 *Opt. Lett.* **46** 4593
[11] Dong P, Yan J, Wang J, *et al*. 2013 *Appl. Phys. Lett.* **102** 241113
[12] Nakarmi M, Kim K, Khizar M, *et al*. 2005 *Appl. Phys. Lett.* **86** 092108
[13] Aman M A H, Noorden A F A, Daud S and Kadir M Z A 2024 *Phys. Scr.* **99** 055557
[14] Nagata K, Matsubara T, Saito Y, *et al*. 2023 *Crystals* **13** 524
[15] Usman M, Malik S, Hussain M, Jamal H and Khan M A 2021 *Opt. Mater.* **112** 110745
[16] Jarman J C, Zhu T, Griffin P H and Oliver R A 2019 *Jpn. J. Appl. Phys.* **58** SCCC14
[17] Wang Q, He L, Wang L, *et al*. 2021 *Opt. Commun.* **478** 126380
[18] Fan X, Sun H, Li X, *et al*. 2015 *Superlattices Microstruct.* **88** 467
[19] Arif R A, Zhao H, Ee Y K and Tansu N 2008 *IEEE J. Quantum Electron.* **44** 573
[20] Shi L, Du P, Tao G, *et al*. 2021 *Superlattices Microstruct.* **158** 107020
[21] Bashir J, Usman M, Ali S and Mustafa L 2025 *J. Inf. Display* **26** 19
[22] Kneissl M, Kolbe T, Chua C, *et al*. 2010 *Semicond. Sci. Technol.* **26** 014036
[23] Amano H, Baines Y, Beam E, *et al*. 2018 *J. Phys. D: Appl. Phys.* **51** 163001
[24] Moustakas T D and Paiella R 2017 *Rep. Prog. Phys.* **80** 106501
[25] Park J S, Kim J K, Cho J and Seong T Y 2017 *ECS J. Solid State Sci. Technol.* **6** Q42
[26] Bashir J, Usman M, Arteev D S and Saeed W 2025 *J. Inf. Display* **26** 149
[27] Pandey A, Shin W, Gim J, *et al*. 2020 *Photonics Res.* **8** 331
[28] Zhang Y, Krishnamoorthy S, Akyol F, *et al*. 2016 *Appl. Phys. Lett.* **109** 121102
[29] Yu H, Ren Z, Memon M H, *et al*. 2021 *Chin. Opt. Lett.* **19** 082503
[30] Lu Y, Guo Y, Liu Z, *et al*. 2024 *Appl. Phys. Lett.* **124** 111102
[31] Neugebauer S, Hoffmann M, Witte H, *et al*. 2017 *Appl. Phys. Lett.* **110** 101103
[32] Usman M, Saba K, Han D P and Muhammad N 2018 *Superlattices Microstruct.* **113** 585
[33] Kudrawiec R and Hommel D 2020 *Appl. Phys. Rev.* **7** 041314